Impact of hole polaron formation on excitonic transitions in MgO from first principles

A. Sameer Nabi [1] and Sahar Sharifzadeh [1,2,*]

[1]Division of Materials Science and Engineering, Boston University, Boston, Massachusetts 02215, USA
[2]Department of Electrical and Computer Engineering, Boston University, Boston, Massachusetts 02215, USA

(Received 11 June 2025; revised 16 October 2025; accepted 21 November 2025; published 18 December 2025)

We present a first-principles investigation of the excitonic properties of magnesia (MgO), an ionic insulator known to host hole polarons. We combine a density functional theory-based approach for structural relaxation in the presence of the hole and many-body perturbation theory to describe the excitonic properties. We determine that the hole polaron introduces new in-gap occupied states 0.6–0.8 eV above the valence band maximum that lead to two low-energy peaks in the optical spectrum. The predicted redshift of the lowest-energy transition due to polaron formation of 0.8 eV agrees well with the experimental Stokes shift of 0.8–0.9 eV. Analysis of the exciton wave function indicates that the electron-hole pair consists of a localized hole and delocalized electron, but that the wave function retains its Wannier-Mott character even in the presence of the hole polaron. Our study demonstrates that combining these previously established methods allows for a relatively computationally inexpensive approach to studying the exciton polaron in materials where only one charge carrier forms a polaron.

DOI: 10.1103/mpb2-3wrb

I. INTRODUCTION

A polaron is a quasiparticle that forms when an excess charge carrier strongly interacts with surrounding lattice vibrations (phonons), resulting in localization of the charge carrier [1–4]. Electron-phonon interactions can also result in the localization of neutral electron-hole pairs or excitons leading to self-trapping [5,6] or the formation of excitonic polarons [7–9]. This localization results in new excitonic states [5,10] that in turn impact the behavior of these materials. Thus, polaron formation impacts electro-optical technologies such as photovoltaics [11], light-emitting diodes [12], and photocatalysts [13], motivating studies of the microscopic mechanisms through which polarons influence optical phenomena [14–16].

Computational modeling of exciton polarons can provide the necessary microscopic insight into the physical properties of polarons but can be computationally challenging as it requires accurate modeling of the structural rearrangement of atoms upon photoexcitation. Within first-principles methods, density functional theory (DFT) can approximate polaron formation and its impact on the electronic properties of materials. DFT-based simulations have been utilized for an accurate description of structural relaxation in the presence of a localized charge carrier, polaron formation energies, wave-function localization due to electron-phonon interactions, and polaron transport [17–24]. To describe exciton self-trapping, i.e., structural relaxation in the presence of a neutral exciton, it is essential to move beyond ground state DFT. While wave-function-based quantum chemistry approaches, such as coupled cluster theory, can be used to study of self-trapped excitons (e.g., in α-quartz [25]), this approach is limited in the size of the clusters that can be studied.

More recently, many-body perturbation theory (MBPT)-based methods have been developed to investigate self-trapped excitons in solids [8,26–30]. MBPT-derived exciton-phonon matrix elements have been utilized in the simulation of phonon-assisted photoluminescence in bulk hexagonal boron nitride (h-BN) [29], and exciton-phonon transition rates in MoS_2 and $MoSe_2$ [30]. In addition, an approximation to excited-state forces within the GW and Bethe-Salpeter equation (BSE) approach has enabled the prediction of self-trapped exciton formation in photoexcited carbon dioxide, α-quartz [26,31], and LiF [28]. A recently introduced supercell free formalism within GW/BSE has allowed the study of exciton polarons in larger systems such as Cs_2ZrBr_6 [7,27] and $CrBr_3$ [8]. Despite these advancements, these methods remain computationally intensive and require multiple BSE calculations, making the use of a DFT formalism appealing.

Here, we investigate the formation of the hole polaron and its impact on the exciton in rocksalt MgO. Cathodoluminescence (CL) measurements on MgO reveal a broad emission band at 6.8–6.9 eV that is distinct from the near-band-edge free-exciton emission at 7.65 eV [32–34] and has been attributed to radiative recombination from self-trapped excitons. Self-trapping of the exciton is hypothesized to originate from the formation of a self-trapped hole polaron [35], which is characterized by localization of the hole on a single oxygen site accompanied by local lattice distortion [20]. Prior DFT-based studies on the self-trapped hole polaron in MgO have investigated the polaron formation energy and associated structural distortions [17], as well as the impact of polaron formation on carrier trapping and electronic transport [35]. These studies have established that the hole polaron is energetically favorable in MgO and significantly modifies the electronic structure.

*Contact author: ssharifz@bu.edu

Building on this foundation, we study the self-trapping of the exciton within MgO due to the formation of the self-trapped polaron. We treat the self-trapped exciton structure as predominantly dictated by the hole polaron, i.e., we assume the structural distortion is driven by the localized hole while the electron remains relatively delocalized. We utilize the recently developed Δ self-consistent field (Δ-SCF) approach described in Ref. [20] to obtain the structural relaxation upon hole polaron formation. We then apply many-body perturbation theory to compute the excited state properties of this relaxed polaron structure. We predict that the lattice distortion associated with polaron formation introduces localized oxygen $2p$ states above the valence band maximum that give rise to new excitonic transitions below the absorption onset. The resulting optical spectrum displays subgap features that closely match the experimental luminescence peaks observed around 6.8–6.9 eV [32,33]. Interestingly, by analysis of the electron-hole correlation function, we determine that the exciton maintains its Wannier-Mott character with little disruption to the hydrogenic wave function in the presence of the polaron. This is because while the hole is localized on a singly oxygen atom, the electron density remains delocalized. Our results highlight the significance of considering polaron formation and the related geometry relaxation when interpreting the luminescence response of MgO. Additionally, we demonstrate a relatively computationally inexpensive approach for the description of the exciton polaron for materials where only one carrier (electron or hole) forms a polaron.

II. COMPUTATIONAL DETAILS

We studied MgO in the rocksalt crystal structure (space group $Fm\bar{3}m$) with initial atomic coordinates obtained from the Materials Project Database [36]. Density functional theory (DFT) calculations within the generalized gradient approximation (GGA) of Perdew, Burke, and Ernzerhof (PBE) [37] were then performed to optimize the structure with and without the presence of the hole polaron. The QUANTUM ESPRESSO software package [38] was utilized with core and nuclei of atoms described with optimized norm-conserving Vanderbilt (ONCV) pseudopotentials [39] taken from the PSEUDODOJO library [40], with 10 and 6 electrons considered valence for Mg and O atoms, respectively. A plane-wave energy cutoff of 90 Ry and a $5 \times 5 \times 5$ Γ-centered uniform k-point grid were used to converge total energies within 1 meV/atom. Atomic positions and lattice parameters of the pristine MgO crystal were optimized until the forces on all atoms were less than 1 meV/Å.

To study the self-trapped hole polaron formation and obtain geometry distortions in the presence of the hole polaron, we constructed a $2 \times 2 \times 2$ (64-atom) supercell of MgO and adopted the procedure outlined by Ref. [20] . In short, within this Δ-SCF based method, we relaxed the atomic structure in the presence of the hole by introducing a single hole (+1 charge) with a weak local potential γ added to the Kohn-Sham Hamiltonian to mitigate self-interaction and derivative discontinuity errors; γ is determined self-consistently until piecewise linearity with respect to the occupation levels is satisfied. The MgO hole polaron structure was presented in Ref. [20] and our results agree well with the published work. As expected, the addition of an electron carrier did not result in structural relaxation or polaron formation. The reason for this is that the valence band is composed of oxygen p-type orbitals, while the conduction band is a delocalized sp-type band.

Quasiparticle energies and optical absorption properties for both the undistorted and hole-polaron structures were computed within the GW/BSE approximation using the BERKELEYGW package [41]. For both structures, calculations were performed on a $2 \times 2 \times 2$ supercell of MgO, which was found to be necessary to encompass the hole polaron. Initial orbitals and energies were taken from DFT-PBE calculations and a one-shot G_0W_0 correction was applied to the DFT eigenvalues. The static dielectric function was computed within the random phase approximation (RPA) [42] and extended to finite frequency using the Generalized Plasmon Pole (GPP) model of Hybertsen and Louie [43]. The dielectric function and quasiparticle energies were calculated with a 50 Ry dielectric function cutoff and 15 000 unoccupied states such that the highest unoccupied state was >400 eV above the valence band maximum (VBM). For the unoccupied states, 5000 bands were calculated within standard DFT, and an additional 10 000 bands were generated using the parabands subroutine of BERKELEYGW. These parameters are consistent with previously reported GW/BSE studies of MgO [44]. The band structure of the supercell was unfolded using the Band Structure Unfolding (BSU) technique, as described by Popescu *et al.* [45], implemented within the QUANTUM ESPRESSO suite. Excitonic properties were obtained by solving the BSE constructed with 20 valence and 8 conduction bands on a $12 \times 12 \times 12k$ grid interpolated from $3 \times 3 \times 3$ k grid with 35 valence and 47 conduction bands in the coarse grid. The imaginary component of the dielectric function was broadened using a Gaussian broadening of 0.05 eV.

To investigate the spatial localization of excitons, we employed the electron-hole correlation function (ECF) analysis of Refs. [46,47]. The ECF is defined as

$$\mathscr{F}_e(\mathbf{r}) = \int |\Psi(\mathbf{r}_e = \mathbf{r} + \mathbf{r}_h, \mathbf{r}_h)|^2 d^3\mathbf{r}_h, \tag{1}$$

where $\mathbf{r}_e$ and $\mathbf{r}_h$ represent electron and hole coordinates, respectively, and the integrals are evaluated over the entire crystal volume. The numerical integration was carried out by summing contributions from 100 discrete hole and electron positions [see Supplemental Material (SM) Sec. II for convergence studies [48]]. In addition to Eq. (1), we also considered the electron-hole correlation function with the electronic coordinates integrated out, i.e.,

$$\mathscr{F}_h(\mathbf{r}) = \int |\Psi(\mathbf{r}_h = \mathbf{r}_e - \mathbf{r},\ \mathbf{r}_e)|^2 d^3\mathbf{r}_e. \tag{2}$$

For $\mathscr{F}_e(\mathbf{r})$, hole positions were sampled around a central oxygen atom within a radius of 1 Å, while for $\mathscr{F}_h(\mathbf{r})$ electron positions were sampled within 1 Å of both Mg and O atoms because of the mixed character of the conduction band (see SM Sec. III for character of bands [48]). This distance is about half of the Mg-O bond length of 2.1 Å.

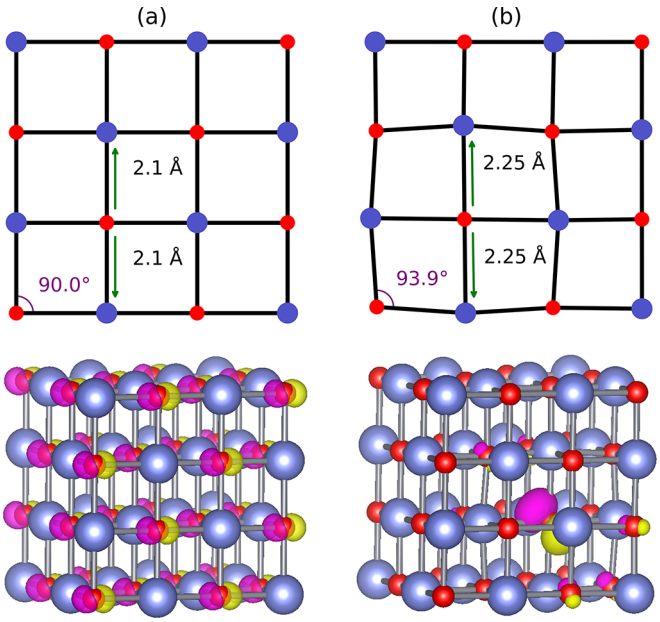

FIG. 1. (a) The Top shows the (*ab*) plane of undistorted MgO with valence band maximum (VBM) orbital density shown at the bottom. (b) Same as (a) for the MgO structured distorted due to the presence of the self-trapped hole polaron.

III. RESULTS

The structure of MgO with and without distortion due to polaron formation is shown in Figs. 1(a) and 1(b). The distortion is mainly localized near one oxygen atom, consistent with Ref. [20]. The bonds near the oxygen atom are stretched and the bond angle with neighboring Mg atoms is distorted away from 90°. As shown in the density plots in Fig. 1, the valence orbital is localized on the oxygen atom, indicating small polaron formation. We note that we also considered the structural relaxation in the presence of an added electron to MgO but found little distortion and no polaron formation, consistent with prior prediction [49].

To understand how observable electronic properties are impacted by polaron formation, we plot the calculated band structure and imaginary component of the dielectric function for both structures in Fig. 2. In the absence of polaron formation, we predict a fundamental gap of 7.9 eV at $\mathbf{k} = \Gamma$ as shown in Fig. 2(a), in good agreement with 7.8 eV extracted from thermoreflectance spectroscopy [50]. The effective mass associated with the valence and conduction bands are $4.55m_e$ and $0.33m_e$, respectively, indicating a heavy hole, and in good agreement with previous first-principles calculations on MgO [44]. Upon hole polaron formation, three additional occupied bands are introduced at 0.64–0.76 eV above the VBM of the undistorted MgO. These bands are nondispersive, as

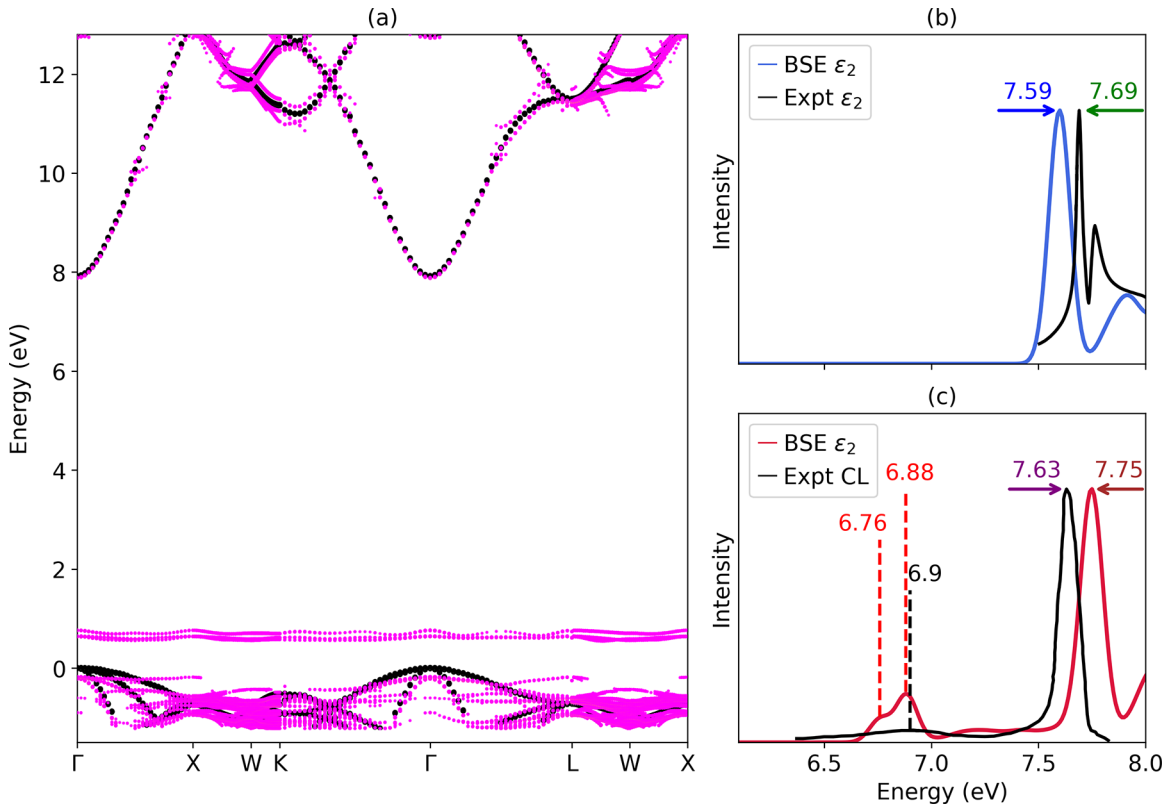

FIG. 2. (a) GW-predicted band structure of MgO for the pristine lattice (black) and the lattice in the presence of a self-trapped hole polaron (pink). (b) and (c) Show the calculated imaginary component of the dielectric function. (b) shows the predicted spectrum without polaron formation (blue) and is compared with experimental optical absorption (black), while (c) shows the predicted spectrum in the presence of a polaron (red) and is compared against experimental cathodoluminescence (black). To aid comparison, intensities in (b) and (c) have been normalized such that the highest intensity peaks are at one.

demonstrated in Fig. S7. As discussed previously [20,35], they are of oxygen $2p$ character and result from the symmetry breaking of the MgO crystal lattice in the presence of the hole polaron.

The structural distortions induced by hole polaron formation in MgO give rise to new optical transitions in the imaginary component of the dielectric function as shown in Figs. 2(b) and 2(c). Without the presence of a polaron, we predict a bright low-energy exciton with absorption onset at 7.6 eV, in good agreement with the experimental onset of 7.7 eV [51]. Hole polaron formation redshifts the absorption onset by 0.84 eV with multiple states contributing to two peaks below the undistorted MgO gap. The lowest-energy peak at 6.76 eV corresponds to transitions from the highest occupied polaron state to the pristine-like MgO conduction band minimum (CBM), while a second peak at 6.88 eV arises from transitions from the two degenerate lower energy polaronic states [shown in Fig. 2(a)] to the CBM (see SM Tables S2 and S3). This finding agrees well with experimental CL measurements, which report broad, low-intensity peaks at 6.8 eV [33] to 6.9 eV [32]. These features were previously attributed to radiative decay from a self-trapped exciton [32], which our calculations agree with. Specifically, we determine that the lattice distortions accompanying polaron formation localize or trap the hole, leading to new optical transitions below the absorption onset. We note that the breaking of translational symmetry and not point group symmetry leads to these new states.

While the energy and intensity of the optical transitions are modified significantly upon polaron formation, the exciton binding energies are within tens of meV for both structures; the binding energy of the lowest-energy excitonic state is 320 meV for unperturbed MgO and 353 meV for the distorted geometry. The similarity in binding energies despite hole localization can be understood within the Wannier-Mott model for which the exciton binding energy can be approximated as $E_b = (\epsilon^2/\mu)^*$ Ry, where $\mu = \frac{m_e^* m_h^*}{m_e^* + m_h^*}$ is the reduced mass and ϵ is the dielectric permittivity. We predict the electronic component of $\epsilon = 3.0\epsilon_0$ with and without the presence of the polaron and μ is also unchanged because it is dominated by the electron mass ($m_e = 0.33m_0$), which is significantly smaller the hole mass $m_h = 4.55m_0$ in pristine MgO. We note that our predicted exciton binding energy is larger than found experimentally (80 meV [34,51] and 145 meV [50]). The discrepancy between our calculated values and these experimental measurements can be attributed primarily to the effects of phonon screening [44] and exciton-phonon coupling, which are not fully captured in the current theoretical approach.

We next investigate the impact of polaron formation on the exciton wave function. In the absence of hole polaron formation, the exciton in MgO is expected to exhibit Wannier-Mott character, with a hydrogenic envelope function describing the correlated behavior of electron and hole. This is owing to the dispersive nature of the VBM and CBM, leading to electron and hole separation greater than the lattice vector. We have previously introduced an analysis of the exciton wave function, via the ECF [46,47], which relates to the envelope function of the exciton and from which the Bohr radius can be extracted. To better understand the exciton wave function in MgO, we apply this analysis technique here.

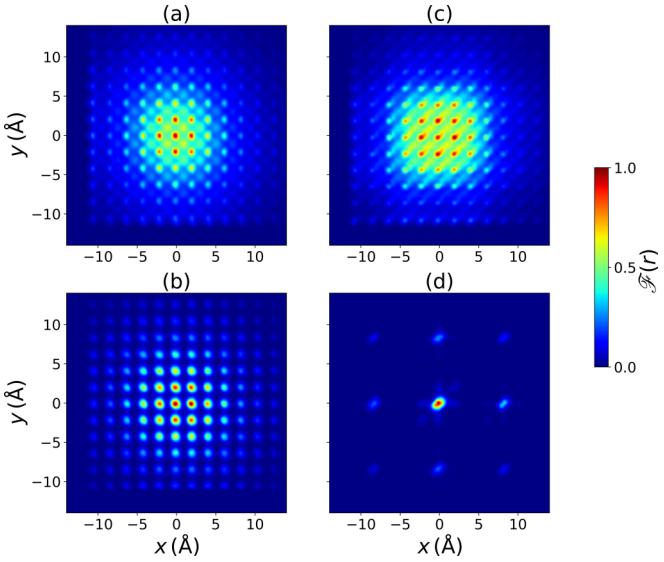

FIG. 3. The electron-hole correlation function associated with the lowest-energy exciton within (a), (b) undistorted and (c), (d) polaron-distorted MgO. (a) and (c) plot the function with the hole coordinate integrated out [Eq. (1)] while (b) and (d) plot Eq. (2).

Figures 3(a) and 3(b) present the ECF of undistorted MgO in two dimensions, with one axis integrated out. There are three nearly degenerate oxygen p-type valence states resulting in three nearly degenerate excitonic states; here, we plot the lowest-energy state with all three shown in Fig. S5 of the SM. Both $\mathscr{F}_e(\mathbf{r})$ [Eq. (1)] and $\mathscr{F}_h(\mathbf{r})$[Eq. (2)] are spherical (Fig. 3), consistent with a Wannier-Mott exciton in the $1s$ state. The average electron-hole distance, calculated as $\langle r \rangle = \int_{\mathbb{R}^3} |\mathbf{r}| \mathscr{F}(\mathbf{r}) d^3\mathbf{r}$, is 8.8 Å, greater than the lattice constant of 4.25 Å (see Table I). As expected from a hydrogenic wave function, the spatial distributions of $\mathscr{F}_e(\mathbf{r})$ and $\mathscr{F}_h(\mathbf{r})$ are nearly identical.

Next, we consider the distortion of the exciton wave function upon polaron formation. The 2D projections of the electron and hole densities for the lowest-energy state are shown in Figs. 3(c) and 3(d). For this system, there is a significant difference between $\mathscr{F}_e(\mathbf{r})$ and $\mathscr{F}_h(\mathbf{r})$. While $\mathscr{F}_e(\mathbf{r})$ is nearly identical to the undistorted system, $\mathscr{F}_h(\mathbf{r})$ is significantly localized. This is because hole polaron formation does not significantly alter the conduction band dispersion but localizes the valence band wave function, leading to this asymmetry. As seen in Table I, the average electron-hole distance associated with $\mathscr{F}_h(\mathbf{r})$ in the distorted geometry is

TABLE I. Computed average electron-hole distances ($\langle|\mathbf{r}|\rangle$) for the electron-hole correlation function and the predicted Bohr radius (a_B) of the envelope function.

Geometry	$\langle\|\mathbf{r}\|\rangle$ (Å)	a_B (Å)
Without polaron (e)	8.9	9.1
Without polaron (h)	8.8	9.2
With self-trapped polaron (e)	8.2	9.6
With self-trapped polaron (h)	2.2	10.2

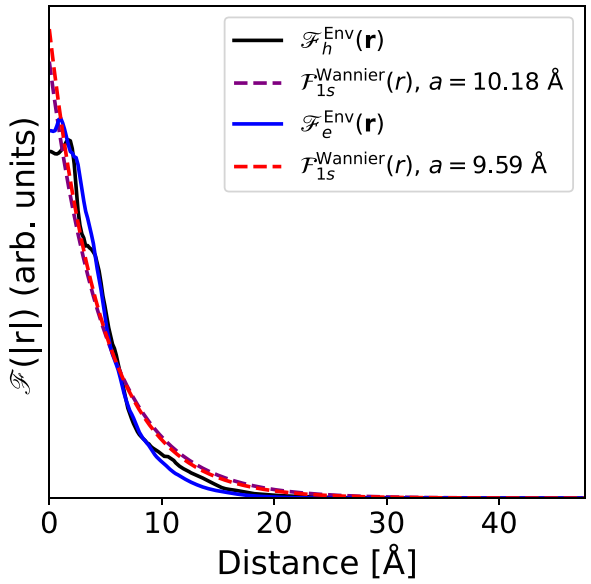

FIG. 4. Envelope of the ECF in the presence of the polaron with envelope of both $\mathscr{F}_h(\mathbf{r})$ and $\mathscr{F}_e(\mathbf{r})$ shown.

∼2.2 Å, which is smaller than the lattice parameter and a quarter of spatial distribution of the electron density.

While the hole density is localized, the nature of the exciton envelope function retains the Wannier-Mott character. We demonstrate this with the envelope of the ECF for the polaron structure shown in Fig. 4. We have previously shown this function is analogous to the exciton envelope function and its spatial decay can be fit to extract the Bohr radius of the exciton [47]. The asymmetry between $F_e(r)$ and $F_h(r)$ in the polaron geometry arises because these correlation functions retain the Bloch periodicity and symmetry of their respective single-particle wave functions. The hole wave function, localized on a single oxygen atom, has lost the cubic symmetry of the pristine lattice, while the electron wave function remains delocalized and symmetric. However, the envelope of the these correlation functions obtained by dividing out the the noninteracting Bloch contributions, reveal the relative coordinate motion of the electron-hole pair and recovers the symmetry between electron and hole. For MgO without polaron formation, fitting the decay function of the $\mathscr{F}(\mathbf{r})$ to obtain the Bohr radius, we find a radius of 9 Å (see SM Sec. II [48] and Table I), slightly larger than 6.1 Å, as expected from the effective mass approximation [44]. In the presence of the hole polaron, the exciton envelope function does not show asymmetry between electron and hole with a fit Bohr radius of 9.5 and 10.1 Å, respectively, indicating that the exciton retains its Wannier-Mott character despite the underlying single-particle asymmetry.

IV. CONCLUSION

In summary, we employed Δ-SCF and many-body perturbation theory to investigate how hole polaron formation impacts the optical properties of rocksalt MgO. Our findings indicate that the structural relaxation and symmetry breaking, caused by the presence of the hole polaron in MgO, introduce new electronic states above the VBM that in turn result in optical transitions below the onset of absorption. Our findings link the observed low-energy PL peaks to structural distortions and new electronic in-gap states due to polaron formation with a predicted Stokes shift due to polaron formation within 0.1 eV of experiment. Additionally, by analysis of the exciton wave function, we found that self-trapping leads to an asymmetry between the electron and hole wave function, with a localized hole and delocalized electron density. However, the exciton wave function retains its Wannier-Mott-like character.

ACKNOWLEDGMENTS

We thank Prof. Jeffrey Neaton (University of California, Berkeley), Prof. Massimiliano Di Ventra (University of California, San Diego), and Dr. Stefano Falletta (Harvard University) for their helpful discussions. We thank Prof. Zhenglu Li (University of Southern California) for providing the code for computing the hole density for fixed electron positions within the BERKELEYGW package. We acknowledge financial support from the U.S. Department of Energy (DOE), Office of Science, Basic Energy Sciences under Award No. DE-SC0023402. We would like to acknowledge computational resources from the Shared Computing Cluster which is administered by Boston University's Research Computing located at the Massachusetts Green High Performing Center (MGHPC) and the National Energy Research Scientific Computing Center (NERSC), a DOE Office of Science User Facility supported by the Office of Science of the U.S. Department of Energy under Contract No. DE-AC02-05CH11231.

DATA AVAILABILITY

The data that support the findings of this article are openly available [52]. The GW-predicted band structures (Fig. 2) are available from the authors upon reasonable request.

[1] L. D. Landau, Electron motion in crystal lattices, Phys. Z. Sowjetunion **3**, 664 (1933).
[2] D. Emin, *Polarons*, 1st ed. (Cambridge University Press, Cambridge, UK, 2012).
[3] A. S. Alexandrov and N. F. Mott, *Polarons and Bipolarons* (World Scientific, Singapore, 1996).
[4] C. Franchini, M. Reticcioli, M. Setvin, and U. Diebold, Polarons in materials, Nat. Rev. Mater. **6**, 560 (2021).
[5] R. T. Williams and K. S. Song, The self-trapped exciton, J. Phys. Chem. Solids **51**, 679 (1990).
[6] W. B. Fowler, M. J. Marrone, and M. N. Kabler, Theory of self-trapped exciton luminescence in halide crystals, Phys. Rev. B **8**, 5909 (1973).
[7] Z. Dai, C. Lian, J. Lafuente-Bartolome, and F. Giustino, Theory of excitonic polarons: From models to first-principles calculations, Phys. Rev. B **109**, 045202 (2024).

[8] Y. Bai, Y. Wang, and S. Meng, *Ab Initio* self-trapped excitons, Phys. Rev. Lett. **133**, 046903 (2024).

[9] S. Biswas, R. Zhao, F. Alowa, M. Zacharias, S. Sharifzadeh, D. F. Coker, D. S. Seferos, and G. D. Scholes, Exciton polaron formation and hot-carrier relaxation in rigid Dion–Jacobson-type two-dimensional perovskites, Nat. Mater. **23**, 937 (2024).

[10] W. Tao, C. Zhang, Q. Zhou, Y. Zhao, and H. Zhu, Momentarily trapped exciton polaron in two-dimensional lead halide perovskites, Nat. Commun. **12**, 1400 (2021).

[11] H. Zhang and N.-G. Park, Polarons in perovskite solar cells: Effects on photovoltaic performance and stability, J. Phys.: Energy **5**, 024002 (2023).

[12] K. Yang, D. Kwon, S. Nam, J. Kim, Y. S. Chung, H. Yoo, I. Park, Y. Park, J. W. Kim, and J. Lee, Interfacial exciton-polaron quenching in organic light-emitting diodes, Phys. Rev. X **14**, 041009 (2024).

[13] Z. Ren, Z. Shi, H. Feng, Z. Xu, and W. Hao, Recent progresses of polarons: Fundamentals and roles in photocatalysis and photoelectrocatalysis, Adv. Sci. **11**, 2305139 (2024).

[14] S. Marcinkevičius and J. S. Speck, Ultrafast dynamics of hole self-localization in β-Ga_2O_3, Appl. Phys. Lett. **116**, 132101 (2020).

[15] K. Miyata, D. Meggiolaro, M. T. Trinh, P. P. Joshi, E. Mosconi, S. C. Jones, F. D. Angelis, and X.-Y. Zhu, Large polarons in lead halide perovskites, Sci. Adv. **3**, e1701217 (2017).

[16] S. Watanabe, K. Ando, K. Kang, S. Mooser, Y. Vaynzof, H. Kurebayashi, E. Saitoh, and H. Sirringhaus, Polaron spin current transport in organic semiconductors, Nat. Phys. **10**, 308 (2014).

[17] S. Kokott, S. V. Levchenko, P. Rinke, and M. Scheffler, First-principles supercell calculations of small polarons with proper account for long-range polarization effects, New J. Phys. **20**, 033023 (2018).

[18] W. H. Sio, C. Verdi, S. Poncé, and F. Giustino, *Ab initio* theory of polarons: Formalism and applications, Phys. Rev. B **99**, 235139 (2019).

[19] M. Reticcioli, U. Diebold, and C. Franchini, Modeling polarons in density functional theory: Lessons learned from TiO_2, J. Phys.: Condens. Matter **34**, 204006 (2022).

[20] S. Falletta and A. Pasquarello, Polarons free from many-body self-interaction in density functional theory, Phys. Rev. B **106**, 125119 (2022).

[21] J. Lafuente-Bartolome, C. Lian, W. H. Sio, I. G. Gurtubay, A. Eiguren, and F. Giustino, *Ab initio* self-consistent many-body theory of polarons at all couplings, Phys. Rev. B **106**, 075119 (2022).

[22] J. Lafuente-Bartolome, C. Lian, W. H. Sio, I. G. Gurtubay, A. Eiguren, and F. Giustino, Unified approach to polarons and phonon-induced band structure renormalization, Phys. Rev. Lett. **129**, 076402 (2022).

[23] Z. Wang, C. Brock, A. Matt, and K. H. Bevan, Implications of the DFT+U method on polaron properties in energy materials, Phys. Rev. B **96**, 125150 (2017).

[24] N. Adelstein, J. B. Neaton, M. Asta, and L. C. De Jonghe, Density functional theory based calculation of small-polaron mobility in hematite, Phys. Rev. B **89**, 245115 (2014).

[25] R. V. Ginhoven, H. Jónsson, K. A. Peterson, M. Dupuis, and L. R. Corrales, An *ab initio* study of self-trapped excitons in α-quartz, J. Chem. Phys. **118**, 6582 (2003).

[26] S. Ismail-Beigi and S. G. Louie, Self-trapped excitons in silicon dioxide: Mechanism and properties, Phys. Rev. Lett. **95**, 156401 (2005).

[27] Z. Dai, C. Lian, J. Lafuente-Bartolome, and F. Giustino, Excitonic polarons and self-trapped excitons from first-principles exciton-phonon couplings, Phys. Rev. Lett. **132**, 036902 (2024).

[28] R. R. Del Grande, and D. A. Strubbe, Revisiting *ab-initio* excited state forces from many-body Green's function formalism: Approximations and benchmark, arXiv:2502.05144.

[29] H.-Y. Chen, D. Sangalli, and M. Bernardi, Exciton-phonon interaction and relaxation times from first principles, Phys. Rev. Lett. **125**, 107401 (2020).

[30] F. Paleari and A. Marini, Exciton-phonon interaction calls for a revision of the "exciton" concept, Phys. Rev. B **106**, 125403 (2022).

[31] S. Ismail-Beigi and S. G. Louie, Excited-State forces within a first-principles green's function formalism, Phys. Rev. Lett. **90**, 076401 (2003).

[32] Z. A. Rachko and J. A. Valbis, Luminescence of free and relaxed excitons in MgO, Phys. Status Solidi B **93**, 161 (1979).

[33] T. Onuma, W. Kosaka, K. Kudo, Y. Ota, T. Yamaguchi, K. Kaneko, S. Fujita, and T. Honda, Identification of free and bound exciton emission of MgO single crystal in vacuum ultraviolet spectral range, Appl. Phys. Lett. **119**, 132105 (2021).

[34] E. Feldbach, I. Kuufmann, and G. Zimmerer, Excitons and edge luminescence in MgO, J. Lumin. **24**, 433 (1981).

[35] J. B. Varley, A. Janotti, C. Franchini, and C. G. Van de Walle, Role of self-trapping in luminescence and p-type conductivity of wide-band-gap oxides, Phys. Rev. B **85**, 081109(R) (2012).

[36] A. Jain, S. P. Ong, G. Hautier, W. Chen, W. D. Richards, S. Dacek, S. Cholia, D. Gunter, D. Skinner, G. Ceder, and K. A. Persson, Commentary: The materials project: A materials genome approach to accelerating materials innovation, APL Mater. **1**, 011002 (2013).

[37] J. P. Perdew, K. Burke, and M. Ernzerhof, Generalized gradient approximation made simple, Phys. Rev. Lett. **77**, 3865 (1996).

[38] P. Giannozzi, S. Baroni, N. Bonini, M. Calandra, R. Car, C. Cavazzoni, D. Ceresoli, G. L Chiarotti, M. Cococcioni, I. Dabo, A. Dal Corso, S. D. Gironcoli, S. Fabris, G. Fratesi, R. Gebauer, U. Gerstmann, C. Gougoussis, A. Kokalj, M. Lazzeri, L. Martin-Samos *et al.*, QUANTUM ESPRESSO: A modular and open-source software project for quantum simulations of materials, J. Phys.: Condens. Matter **21**, 395502 (2009).

[39] D. R. Hamann, Optimized norm-conserving Vanderbilt pseudopotentials, Phys. Rev. B **88**, 085117 (2013).

[40] M. J. V. Setten, M. Giantomassi, E. Bousquet, M. J. Verstraete, D. R. Hamann, X. Gonze, and G.-M. Rignanese, The PSEUDODOJO: Training and grading a 85 element optimized norm-conserving pseudopotential table, Comput. Phys. Commun. **226**, 39 (2018).

[41] J. Deslippe, G. Samsonidze, D. A. Strubbe, M. Jain, M. L. Cohen, and S. G. Louie, BERKELEYGW: A massively parallel computer package for the calculation of the quasiparticle and optical properties of materials and nanostructures, Comput. Phys. Commun. **183**, 1269 (2012).

[42] D. M. Ceperley and B. J. Alder, Ground state of the electron gas by a stochastic method, Phys. Rev. Lett. **45**, 566 (1980).

[43] M. S. Hybertsen and S. G. Louie, Electron correlation in semiconductors and insulators: Band gaps and quasiparticle energies, Phys. Rev. B **34**, 5390 (1986).

[44] A. M. Alvertis, J. B. Haber, Z. Li, C. J. N. Coveney, S. G. Louie, M. R. Filip, and J. B. Neaton, Phonon screening and dissociation of excitons at finite temperatures from first principles, Proc. Natl. Acad. Sci. USA **121**, e2403434121 (2024).

[45] V. Popescu and A. Zunger, Extracting *e* versus *k* effective band structure from supercell calculations on alloys and impurities, Phys. Rev. B **85**, 085201 (2012).

[46] S. Sharifzadeh, P. Darancet, L. Kronik, and J. B. Neaton, Low-Energy charge-transfer excitons in organic solids from first-principles: The case of pentacene, J. Phys. Chem. Lett. **4**, 2197 (2013).

[47] D. K. Lewis and S. Sharifzadeh, Defect-induced exciton localization in bulk gallium nitride from many-body perturbation theory, Phys. Rev. Mater. **3**, 114601 (2019).

[48] See Supplemental Material at http://link.aps.org/supplemental/10.1103/mpb2-3wrb for MBPT convergence information, band structure and projected density of states, and more information on the ECF and exciton envelope function of MgO.

[49] B. Guster, P. Melo, B. A. A. Martin, V. Brousseau-Couture, J. C. D. Abreu, A. Miglio, M. Giantomassi, M. Côté, J. M. Frost, M. J. Verstraete, and X. Gonze, Fröhlich polaron effective mass and localization length in cubic materials: Degenerate and anisotropic electronic bands, Phys. Rev. B **104**, 235123 (2021).

[50] R. C. Whited, C. J. Flaten, and W. C. Walker, Exciton thermoreflectance of MgO and CaO, Solid State Commun. **13**, 1903 (1973).

[51] D. M. Roessler and W. C. Walker, Electronic spectrum and ultraviolet optical properties of crystalline MgO, Phys. Rev. **159**, 733 (1967).

[52] A. S. Nabi, GitHub MgO data repository (2025), https://github.com/fpmats/MgO.